NANO LETTERS

2008
Vol. 8, No. 1
173−177

Molecular Doping of Graphene

T. O. Wehling,*,† K. S. Novoselov,‡ S. V. Morozov,§ E. E. Vdovin,§ M. I. Katsnelson,|| A. K. Geim,‡ and A. I. Lichtenstein†

1st Institute for Theoretical Physics, Hamburg University, Jungiusstrasse 9, D-20355 Hamburg, Germany, School of Physics and Astronomy, University of Manchester, M13 9PL, Manchester, U.K., Institute for Microelectronics Technology, 142432 Chernogolovka, Russia, and Institute for Molecules and Materials, Radboud University of Nijmegen, Toernooiveld 1, 6525 ED Nijmegen, The Netherlands

Received September 14, 2007; Revised Manuscript Received November 20, 2007

ABSTRACT

Graphene is considered as one of the most promising materials for post silicon electronics, as it combines high electron mobility with atomic thickness [Novoselov et al. *Science* 2004, *306*, 666–669. Novoselov et al. *Proc. Natl. Acad. Sci. U.S.A.* 2005, *102*, 10451–10453]. The possibility of chemical doping and related excellent chemical sensor properties of graphene have been demonstrated experimentally [Schedin et al. *Nat. Mater.* 2007, *6*, 652–655], but a microscopic understanding of these effects has been lacking, so far. In this letter, we present the first joint experimental and theoretical investigation of adsorbate-induced doping of graphene. A general relation between the doping strength and whether adsorbates are open- or closed-shell systems is demonstrated with the NO_2 system: The single, open shell NO_2 molecule is found to be a strong acceptor, whereas its closed shell dimer N_2O_4 causes only weak doping. This effect is pronounced by graphene's peculiar density of states (DOS), which provides an ideal situation for model studies of doping effects in semiconductors. We show that this DOS is ideal for "chemical sensor" applications and explain the recently observed [Schedin et al. *Nat. Mater.* 2007, *6*, 652–655] NO_2 single molecule detection.

Controlling the type and the concentration of charge carriers is at the heart of modern electronics: it is the ability to combine gate voltages and dopant concentration to locally change the density of electrons or holes that allows the variety of nowadays available semiconductor-based devices. However, according to the semiconductor industry roadmap, the conventional Si-based electronics is expected to encounter fundamental limitations at the spatial scale below 10 nm, thus calling for novel materials that might substitute or complement Si. One possible candidate for the material for future electronics is graphene, the two-dimensional form of carbon with atoms arranged in a honeycomb lattice.[1,2,4] It exhibits ballistic transport on a submicron scale and can be doped heavily, either by gate voltages or molecular adsorbates, without significant loss of mobility.[1,3] These extraordinary transport properties are determined by different sources of scattering, which are a matter of controversy in graphene and carbon nanotubes (CNTs) at the moment. Controlling and discriminating between different scattering channels requires an understanding of doping mechanisms on the atomic level. In addition to electronic applications, recent experiments[3] have demonstrated graphene's potential for solid-state gas sensors and even the possibility of single molecule detection. A clear picture of the physics behind these doping and gas-sensing effects is the central issue of this letter and will allow for the optimization of future gas detection and electronic devices.

Doping in graphene-related systems has attracted a lot of research activity in the past years. Already, the first experiments with graphene showed the possibility of inducing charge carriers to this material by the adsorption of various gases including NH_3, H_2O, and NO_2.[1] Hall effect measurements proved that NH_3 induces electrons, whereas the latter two types of adsorbates result in holes as charge carriers. Those gases have been detected at remarkably low concentrations, and NO_2 has even been detected in the extreme limit of single molecules.[3] CNTs, being rolled up graphene sheets, exhibit similar doping effects upon gas exposure[5] and stimulated first-principles studies of these systems: density functional theory (DFT) calculations for NO_2, H_2O, and NH_3 on nanotubes revealed possible physisorbed geometries on nondefective CNTs and developed a "standard model" to interpret this doping:[6−8] By considering Mulliken or Löwdin charges of the adsorbed molecules, NO_2 is found to accept 0.1 e^- per molecule from the tube, whereas one NH_3 molecule is predicted to donate between 0.03 and 0.04 e^-.[7,8] However, this "standard model" for CNTs fails for graphene, especially in explaining the qualitative difference between NO_2 and the other adsorbates.

* Corresponding author.
† Hamburg University.
‡ University of Manchester.
§ Institute for Microelectronics Technology.
|| Radboud University of Nijmegen.

10.1021/nl072364w CCC: $40.75
Published on Web 12/18/2007

In this work, we have chosen the NO_2 system providing both open-shell single molecules and closed-shell dimers N_2O_4 to study the doping due to adsorbates by combining ab initio theory with transport measurements. Theoretically, the electronic and structural properties of the graphene adsorbate systems are addressed by means of DFT. As van der Waals forces are ill represented in the local density approximation (LDA) as well as in gradient-corrected exchange correlation functionals (GGA) resulting in over- and underbonding, respectively,[9] we apply both functionals to obtain upper and lower bounds for adsorption energies and related structural properties. All calculations are carried out with the Vienna Ab Initio Simulation Package (VASP)[10] using projector augmented waves (PAWs)[11,12] for describing the ion cores. The corresponding plane wave expansions of the Kohn−Sham orbitals were cut off at 875 eV in the GGA[13,14] and at 957 eV in the LDA calculations. In this periodic scheme, single NO_2 and N_2O_4 adsorbates are modeled in 3×3 and 4×4 graphene supercells, respectively. The ionic configurations presented in this letter are fully relaxed, i.e., with all forces being less than 0.02 eV $Å^{-1}$, and the convergence of subsequent total energy calculations is guaranteed by applying the tetrahedron method with Blöchl corrections on Γ-centered k-meshes denser than $30 \times 30 \times 1$, when folded back to the single graphene Brillouin zone. In the spirit of ref 15, the density of states (DOS) values obtained in our DFT calculations are the central quantities in the following discussion of the adsorbate effects on the electronic properties of the graphene sheets.

Gaseous NO_2 stands in equilibrium with its dimer N_2O_4, giving rise to various different adsorption mechanisms on graphene, similar to the case of graphite.[16,17] For both, we obtained possible adsorption geometries as depicted in Figure 1, right. The corresponding adsorption energies in GGA are 85 meV (a), 67 meV (b), 67 meV (c), 50 meV (d), and 44 meV (e) per molecule, with sheet-adsorbate distances of 3.4−3.5 Å for the monomer and 3.8−3.9 Å for the dimer. As usual, LDA yields higher adsorption energies (approximately 169−181 meV for the monomer and 112−280 meV for the dimer) and favors the adsorbates by 0.5−1 Å nearer to the sheet. Adsorption near defects can cause higher adsorption energies, such as, for example, chemisorption of NO_2 at a vacancy defect yielding 1.8 eV. However, the doping effects occurring there turn out to be similar to those on perfect graphene. So we will limit the following discussion to the latter case.

The spin-polarized DOS of the supercells containing NO_2, shown in Figure 1a,b, reveals a strong acceptor level at 0.4 eV below the Dirac point in both adsorption geometries. The molecular orbitals of NO_2 correspond to flat bands and manifest themselves as peaks in the DOS. The energies of these peaks are virtually independent of the adsorbate orientation. Most important for doping effects is the partially occupied molecular orbital (POMO) of NO_2, which is split by a Hund-like exchange interaction: the spin-up component of this orbital is approximately 1.5 eV below the Dirac point and fully occupied, as it is also for the case of free NO_2 molecules. The spin down component of the NO_2 POMO is

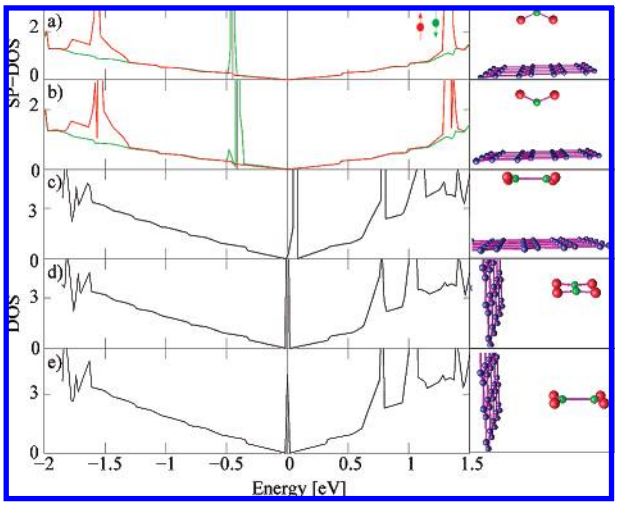

Figure 1. Left: Spin-polarized DOS of the graphene supercells with adsorbed NO_2 (a,b) and DOS of graphene with N_2O_4 (c−e), in various adsorption geometries. The energy of the Dirac points is defined as $E_D = 0$. In the case of NO_2, the Fermi level E_f of the supercell is below the Dirac point, directly at the energy of the spin down POMO, whereas, for N_2O_4, E_f is directly at the Dirac points. Right: Adsorption geometries obtained with GGA. The carbon atoms are printed in blue, nitrogen is shown in green, and oxygen is shown in red.

unoccupied for free NO_2, but is 0.4 eV below the Dirac point in the adsorbed configuration.[25] Hence, it can accept one electron from graphene in the dilute limit, which corresponds to the limit of an infinitely large supercell.

By means of band structure calculations, we investigated the bandwidth and hybridization of the NO_2 acceptor bands with the graphene bands. It turns out that, in a small region, less than 1% of the Brillouin zone, where the graphene and the NO_2 POMO bands come as close as 40 meV, these bands start mixing significantly. In the entire rest of the Brillouin zone, the acceptor band is localized almost entirely at the adsorbate and extends over 5 meV in energy space.

In contrast to the paramagnetic monomer, the dimer, N_2O_4, has no unpaired electrons and is diamagnetic: upon formation from two monomers, the two POMOs hybridize with the resulting bonding orbital being the highest occupied molecular orbital (HOMO). The possibility of doping effects due to adsorbed dimers has been investigated using the DOS depicted in Figure 1c−e. Again, the molecular orbitals of the adsorbates are recognizable as sharp peaks in the supercell DOS. Similar to NO_2, band structure calculations reveal hybridization of the adsorbate and the graphene bands, where these bands come as close as 40 meV, and an impurity bandwidth of about 3 meV outside the band crossing region. One finds that the N_2O_4 HOMO is in all cases more than 3 eV below the Fermi level and therefore does not give rise to any doping. However, the lowest unoccupied molecular orbital (LUMO) is always quite near to the Dirac point, i.e., between 1 and 66 meV above it.[26] Those initially empty N_2O_4 LUMOs can be populated by the graphene electrons as a result of thermal excitations and act consequently as acceptor levels. Thus *both* N_2O_4 and NO_2 give rise to *p*-type doping of graphene, with one decisive distinction: the affinity of the open shell monomer to accept electrons from graphene

is much stronger than that of the dimer. Note that, despite the DOS at the Fermi level being high, neither the dimer nor the monomer are Jahn−Teller active, as there is no orbital degeneracy.

Our theoretical considerations made so far imply the following experimentally checkable features: First, there will be two types of dopants when graphene is exposed to NO_2—the monomer and the dimer—giving rise to acceptor levels far below and rather close to the Dirac point, respectively. Furthermore, we find both acceptor states almost entirely localized at the adsorbate molecules and similarly weakly hybridized with the graphene p_z bands. Therefore electrons in both acceptor states should exhibit a similar electron mobility, which should be much less than the mobility of the electrons in the graphene bands.

These predictions will be examined experimentally in the following part of this letter by combining electric field effect and Hall measurements at different adsorbate concentrations. To this end, we prepared Hall bar devices with Ti/Au (5 nm/40 nm) contacts from monolayer graphene flakes[18] on heavily doped oxidized (300 nm SiO_2) silicon substrate. As prepared, our samples were unintentionally p-doped, likely caused by water on the graphene surface. This unintentional doping was removed by annealing in vacuum for 2 h at 410 K.[1]

Then the samples were exposed to NO_2 strongly diluted in nitrogen (100 ppm of NO_2) for 60 s at room temperature. After the exposure, the chamber was evacuated, and the samples were annealed in a number of annealing cycles while being constantly kept under vacuum. During each annealing cycle our, devices were heated up to 410 K, kept at that temperature for some time, allowing for desorption of some NO_2/N_2O_4 (thus reducing the doping level slightly), and then cooled to room temperature at which longitudinal R_{xx} and Hall R_{xy} resistances were measured at $B = 1$ T as a function of the gate voltage V_G using a standard low-frequency lock-in technique. This procedure allowed us to vary the level of doping gradually in the range from 3×10^{12} cm^{-2} down to practically pristine state with doping as low as 10^{11} cm^{-2} by controlling the time spent at 410 K (varied from 2 min for the very first cycle up to 16 h for the last cycle, when the undoped state was reached). At $T = 300$ K, the level of doping achieved after each of the annealing cycles was stable with the precision of a few percent. Figure 2 presents R_{xy} as a function of the gate voltage for a sample annealed in 16 cycles (though only three measurements[27] taken in the 4th, 7th, and 13th cycles, plus the curve for the pristine state are presented for clarity).

These R_{xy} versus V_G measurements exhibit two characteristic features. First, the curves move toward higher positive gate voltages with increasing NO_2/N_2O_4 doping. Second, the transition region, where R_{xy} depends linearly on the gate voltage (corresponding to the presence of both types of carriers), becomes wider, and, simultaneously, the maximum R_{xy} achieved becomes lower for a higher amount of NO_2/N_2O_4 on the graphene sample. This is clear evidence of the two distinct acceptor levels, as will be explained in the following.

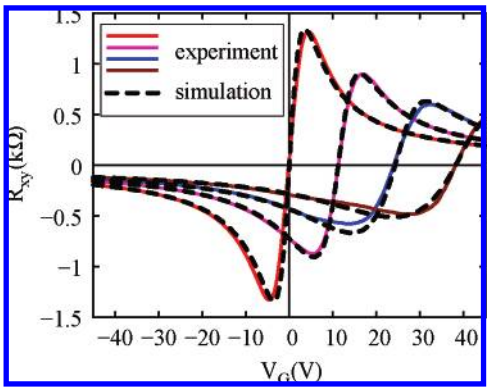

Figure 2. The Hall resistance R_{xy} as a function of the gate voltage V_G for a graphene sample with different levels of NO_2/N_2O_4 doping. The solid lines are the experimental results, with the brown curve corresponding to the highest concentration of adsorbates, and the red curve corresponding to almost zero doping. The dashed lines are the simulations. They are fitted to the experimental curves by adjusting the dopant concentrations c_1 and c_2 for each curve (see text). The simulation close to the red curve corresponds to undoped graphene, $c_1 = c_2 = 0$.

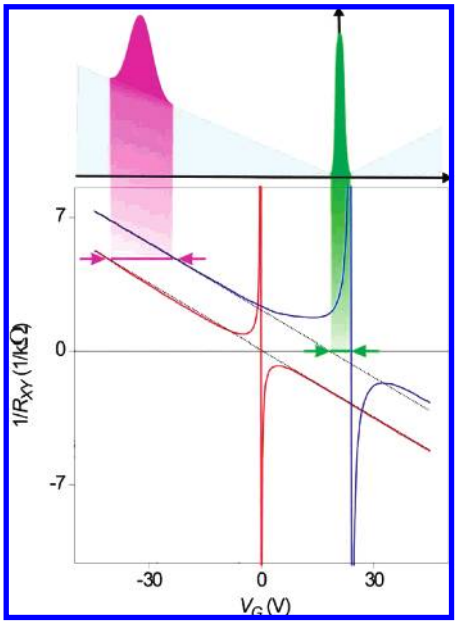

Figure 3. $1/R_{xy}$ for pristine (red curve) and doped (blue curve) graphene samples. Upper panel: the DOS of doped graphene (corresponds to the blue curve), with gray depicting the DOS for pure graphene, the magenta peak representing the DOS for NO_2, and the green peak representing N_2O_4. Shifting of the blue curve with respect to the undoped one (red) suggests the presence of the low-laying NO_2 peak, and the fact that the electron branch for blue curve is shifted with respect to the hole branch indicates the presence of the N_2O_4 peak.

Consider $1/R_{xy}$ as shown in Figure 3. The deep acceptor level causes a solid shift at all V_G, while the acceptor level close to the Dirac point gives rise to an additional shift of the electron branch (straight line at negative $1/R_{xy}$). The curve for doped graphene (blue curve) exhibits these two shifts with respect to the red curve, which corresponds to undoped graphene. The NO_2-acceptor level shifts the entire doped curve to the right, whereas the additional shift of the electron branch reflects the presence of the N_2O_4 impurity level near

the Dirac point. The latter additional shift in $1/R_{xy}$ displays as broadening of the transition region near the charge neutrality point in the R_{xy} curves, as discussed above. We would like to stress that similar behavior can be seen in the R_{xx} curves, where the peak broadens and its position shifts toward higher positive gate voltages. However, here we would like to concentrate on R_{xy} as the most suggestive measurements.

To make the analysis more quantitative, we present a simple model, which is based on the presence of four types of carriers: electrons and holes in graphene as well as electrons in the NO_2 and N_2O_4 acceptor states. Electrons and holes in graphene have approximately the same, rather high mobility of about 5000 cm^2/Vs.[1] Our DFT calculations predict the acceptor bands to both be flat with a similar bandwidth, and a similar, weak hybridization with the graphene bands is found. Thus, we expect the mobility μ of electrons in the impurity states to be much smaller than the mobility of the electrons in the graphene bands. Expressing the impurity-state electron mobility μ in units of the graphene electron mobility, the Hall resistance is given by[19] $R_{xy} = (B(\mu^2 c + n - p)/e(\mu c + n + p)^2)$, where n (p) is the density of electrons (holes) in graphene, and c is the density of electrons in the impurity states. As the gate voltage $V_G = \alpha\sigma$ is directly related to the total charge density of the sample $\sigma = e(c + n - p)$, where the prefactor α is determined by substrate properties as described in ref 1, we can simulate the Hall resistance as a function of V_G.

To this end, we adjust the global fit parameter α to the slope of the $|1/R_{xy}|$ curves. Once the impurity-state electron mobility μ and the impurity DOS N_{imp} are specified, R_{xy} and V_G are functions of the chemical potential, since n, p, and c are determined by the graphene DOS and N_{imp}, respectively, via the Fermi distribution function. It turns out that, for reasonable agreement of *all* 17 experimental curves (four of them presented in Figure 2) with the simulations, $\mu \approx 0.1$ is required and $N_{imp}(E)$ has to be peaked around *two* distinct energies, $E_1 \leq -300$ meV and $E_2 \approx -40$ meV. Taking in particular $N_{imp}(E) = c_1\delta(E - E_1) + c_2\delta(E - E_2)$,[28] we simulate the R_{xy} versus V_G measurements with three global fit parameters α, μ, and E_2 and two curve specific fit parameters, c_1 and c_2. $E_1 \leq -300$ meV corresponds to our DFT estimation of $E_1 \approx -400$ meV. The good agreement of simulations and experiment (see Figure 2) confirms the presence of two distinct impurity levels due to the NO_2 and N_2O_4 as predicted by DFT. The coefficients c_1 and c_2 are the measures of the density of electronic states due to the NO_2 and N_2O_4 adsorbates, respectively. From the fitting of the simulations to the experimental curves we obtain $c_1 =$ 1.7, 1.1, and 0.6 $\times$ 10^{12} cm^{-2} and $c_2 =$ 1.3, 0.9, and 0.3 $\times$ 10^{12} cm^{-2} for the brown, blue, and magenta curve in Figure 2, respectively, corresponding to 3000−10 000 molecules on a device of 0.75 μm $\times$ 0.75 μm in size.

The deep acceptor level at $E_1 \leq -300$ meV due to NO_2 is always fully occupied under our experimental conditions. This full occupancy corresponds to the transfer of *one* electron from graphene sheets to NO_2 per adsorbate molecule, as observed in ref 3. The occupancy of the NO_2 acceptor orbital is basically independent of temperature, which is very different from normal semiconductors, where the acceptor states are inside the gap and populated as a result of thermal excitation. Therefore, graphene electronic devices could be operated at arbitrarily low temperatures, in contrast to usual semiconductor devices.

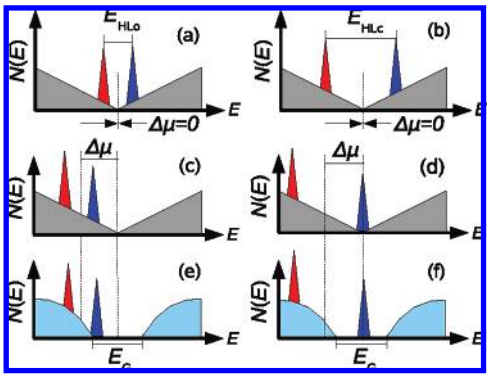

Figure 4. Doping dependence on chemical potential mismatch $\Delta\mu$, HOMO/LUMO splitting E_{HL}, and the host's DOS. The left (right) column corresponds to paramagnetic (nonmagnetic) adsorbates. ($E_{HLo} \ll E_{HLc}$, see text.) The combined DOS, $N(E)$, (before equilibration of the adsorbate's and host's chemical potentials) is shown for graphene (a−d) and a semiconductor with a gap E_G (e,f) as host material. (a,b) $\Delta\mu = 0$. The adsorbate's HOMO (red) and LUMO (blue) are well inside the valence and the conduction bands of the host, respectively, resulting in no doping (also for a semiconductor with a gap, not shown here for brevity). (c) A small mismatch in the chemical potential $\Delta\mu > (1/2)E_{HLo}$ leads to strong doping in the case of a paramagnetic molecule (NO_2) on graphene. (d) A much larger mismatch is required $\Delta\mu > (1/2)E_{HLc}$ to produce acceptor levels in the case of a paramagnetic molecule (N_2O_4) on graphene. (e,f) The mismatch in chemical potential $|\Delta\mu| > (1/2)(E_{HL} + E_G)$, which is required to produce doping in the case of a semiconductor with a gap is much larger than in the case of graphene: (e) corresponds to weak doping and (f) to no doping.

Above, we elaborated on the strong difference between NO_2 and N_2O_4 adsorbates regarding the impurity level energies and the doping strength. We would like to argue that this is a manifestation of a general difference between the doping by paramagnetic and diamagnetic adsorbates. The latter type of impurities act generally as rather weak dopants or do not give rise to any doping at all (Figure 4, right column), whereas the paramagnetic impurities cause strong doping (Figure 4, left column): closed shell molecules are chemically rather inert and exhibit HOMO/LUMO gaps typically on the order of $E_{HLc} \approx 5-10$ eV;[20] for doping by diamagnetic adsorbates, a mismatch of the molecular and the graphene chemical potential in the same order of magnitude or cluster formation is required. For open-shell systems, the situation is the opposite: as one orbital is only partially populated, occupied and unoccupied states are only separated by Hund exchange on the order of $E_{HLo} \approx 1$ eV. Thus, any open-shell molecule will give rise to doping as long as the chemical potential mismatch $\Delta\mu$ between the adsorbate and graphene exceeds half the Hund exchange splitting, i.e., $\Delta\mu \gtrsim 0.5$ eV (see Figure 4). This displays a close relation between graphene's DOS and the fact that this material can be easily doped by many adsorbates. As there is no gap in the spectrum, a small mismatch in the chemical

potential can be sufficient to provide an active donor or acceptor level (see Figure 4). The introduction of a gap in conventional semiconductors means that the chemical potential mismatch has to exceed half the value of the gap in order to achieve any doping. Therefore, graphene gas sensors will, in general, be more sensitive than those built from usual semiconductors.

Flat bands near the Fermi level are an origin of ferromagnetism and many related electronic instabilities. NO_2 molecules adsorbed on graphene create and control the occupancy of flat impurity bands near the Dirac point as well as they can lead to exchange scattering. This warrants future attention, as it can result in strongly spin-polarized impurity states[21] and lead to a possible pathway[22] to high-temperature magnetic order in graphene.

Acknowledgment. This work was supported by SFB 668 (Germany) and FOM (The Netherlands). KSN and AKG are grateful to the Royal Society and EPSRC (UK). SVM and EEV acknowledge RFBR and the "Quantum Macro Physics" program (Russia).

References

(1) Novoselov, K. S.; Geim, A. K.; Morozov, S. V.; Jiang, D.; Zhang, Y.; Dubonos, S. V.; Grigorieva, I. V.; Firsov, A. A. *Science* **2004**, *306*, 666−669.
(2) Novoselov, K. S.; Jiang, D.; Schedin, F.; Booth, T. J.; Khotkevich, V. V.; Morozov, S. V.; Geim, A. K. *Proc. Natl. Acad. Sci. U.S.A.* **2005**, *102*, 10451−10453.
(3) Schedin, F.; Geim, A. K.; Morozov, S. V.; Hill, E. W.; Blake, P.; Katsnelson, M. I.; Novoselov, K. S. *Nat. Mater.* **2007**, *6*, 652−655.
(4) Geim, A. K.; Novoselov, K. S. *Nat. Mater.* **2007**, *6*, 183−191.
(5) Kong, J.; Franklin, N. R.; Zhou, C. W.; Chapline, M. G.; Peng, S.; Cho, K. J.; Dai, H. J. **2000**, *287*, 622−625.
(6) Peng, S.; Cho, K. *Nanotechnology* **2000**, *11*, 57−60.
(7) Chang, H.; Lee, J. D.; Lee, S. M.; Lee, Y. H. *Appl. Phys. Lett.* **2001**, *79*, 3863−3865.
(8) Zhao, J.; Buldum, A.; Han, J.; Lu, J. P. *Nanotechnology* **2002**, *13*, 195−200.
(9) Meijer, E. J.; Sprik, M. *J. Chem. Phys.* **1996**, *105*, 8684−8689.
(10) Kresse, G.; Hafner, J. *J. Phys.: Condens. Matter* **1994**, *6*, 8245−8257.
(11) Kresse, G.; Joubert, D. *Phys. Rev. B* **1999**, *59*, 1758−1775.
(12) Blöchl, P. E. *Phys. Rev. B* **1994**, *50*, 17953−17979.
(13) Perdew, J. P. *Electronic Structure of Solids '91*; Akademie Verlag: Berlin, 1991.
(14) Perdew, J. P.; Chevary, J. A.; Vosko, S. H.; Jackson, K. A.; Pederson, M. R.; Singh, D. J.; Fiolhais, C. *Phys. Rev. B* **1992**, *46*, 6671−6687.
(15) Santucci, S.; Picozzi, S.; Gregorio, F. D.; Lozzi, L.; Cantalini, C.; Valentini, L.; Kenny, J. M.; Delley, B. *J. Chem. Phys.* **2003**, *119*, 10904−10910.
(16) Sjovall, P.; So, S. K.; Kasemo, B.; Franchy, R.; Ho, W. *Chem. Phys. Lett.* **1990**, *172*, 125−130.
(17) Moreh, R.; Finkelstein, Y.; Shechter, H. *Phys. Rev. B* **1996**, *53*, 16006−16012.
(18) Graphene Industries Home Page. www.grapheneindustries.com (accessed September 2007).
(19) Kim, J. S. *J. Appl. Phys.* **1999**, *86*, 3187−3194.
(20) Zhan, C.-G.; Nichols, J.; Dixon, D. *J. Phys. Chem. A* **2003**, *107*, 4184−4195.
(21) Wehling, T. O.; Balatsky, A. V.; Katsnelson, M. I.; Lichtenstein, A. I.; Scharnberg, K.; Wiesendanger, R. *Phys. Rev. B* **2007**, *75*, 125425.
(22) Edwards, D. M.; Katsnelson, M. I. *J. Phys.: Condens. Matter* **2006**, *18*, 7209−7225.
(23) Kim, W.; Javey, A.; Vermesh, O.; Wang, Q.; Li, Y.; Dai, H. *Nano Lett.* **2003**, *3*, 193−198.
(24) Bradley, K.; Cumings, J.; Star, A.; Gabriel, J.-C. P.; Grüner, G. *Nano Lett.* **2003**, *3*, 639−641.
(25) The energies of the POMO spin up and down orbitals relative to the Dirac points predicted by LDA are −0.5eV and −1.4eV, respectively, i.e., in almost quantitative agreement with the GGA results.
(26) LDA locates these LUMOs between 2 meV and 210 meV above the Dirac point.
(27) Hysteretic behavior (in V_G) was observed when visiting large gate voltages (above 40 V) For the sweep rates used in our experiments (15 V/min), the typical hysteresis was 1.5 V; however, it could be as high as 5 V if the time spent at high voltages was too long. Such hysteresis has been discussed in refs 23 and 24, but the exact cause of this effect is beyond the scope of this paper. Here, we always present the data obtained during sweeps from negative to positive voltages (−45 V → +45 V), and we always made sure that the time spent at −45 V was kept at a minimum.
(28) The broadness of the impurity levels does not strongly influence the simulations.

NL072364W